Renewable and Sustainable Energy Reviews 189 (2024) 113963

Contents lists available at ScienceDirect

Renewable and Sustainable Energy Reviews

journal homepage: www.elsevier.com/locate/rser

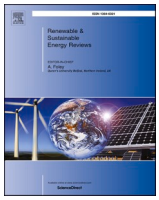

Optimal day-ahead large-scale battery dispatch model for multi-regulation participation considering full timescale uncertainties

Mingze Zhang [a], Weidong Li [a,*], Samson Shenglong Yu [b], Haixia Wang [a], Yu Ba [a]

[a] School of Electrical Engineering, Dalian University of Technology, Dalian, 116024, China
[b] School of Engineering, Deakin University, Melbourne, Victoria, 3216, Australia

ARTICLE INFO

Keywords:
Day-ahead scheduling
Large-scale batteries
Power system economics
Power system reliability
Power system reserve
Renewable energy systems

ABSTRACT

Grid scale battery integration plays an important role in renewable energy integration and the formation of smart grid. To mitigate the problems of insufficient frequency response and peak regulation capacities faced by modern power grids with high wind energy uptake, a day-ahead optimization dispatch strategy considering operational risks is proposed in this study. In the day-ahead dispatch model, generation units and a large-scale battery energy storage station (LS-BESS) are coordinated to participate in multi-type frequency control ancillary services (FCASs). For optimal performance, scheduling in different timescales and the complementarity between power and energy types of requirements are coordinated, with various service uncertainties considered. Then the conditional value-at-risk theory is utilized to achieve the optimal mix of multiple resources for day-ahead regulation reserves, to realize the minimum operation cost. To tackle the uncertainty of wind power over a large timescale, a robust optimization (RO) approach based on the budget uncertainty set is employed, which considers robustness and economy. This can help avoid over-conservation of the standard RO and enhance the applicability of the decisions made. Simulation studies and comparison analysis of multiple schemes verify the effectiveness of the proposed optimal day-ahead dispatch strategy, which also demonstrate that a LS-BESS participating in multiple FCASs for day-ahead dispatch can help realize secure, reliable, and economic power grid.

1. Introduction

Active power regulations in power systems are coordinated by FCASs at different timescales, including inertia frequency response (IFR) and PFR on the timescale of tens of seconds to ensure security, SFR on the timescale of a few minutes to improve quality, and hourly peak regulation to achieve power balance. With growing penetration of renewable energy and gradual decommission of conventional generation units, some issues have arisen for FCASs: 1) power system's IFR and PFR are weakened [1,2], so its resilience to resist step disturbances is diminished, and the risk of load shedding is increased; 2) SFR is weakened [3], which reduces the flexibility of the power system to deal with load and wind power fluctuations, leading to possible frequency instability; and 3) the anti-peak regulation characteristic of wind power [4] deteriorates the downward peak shaving capacity [5], and wind energy has high uncertainty, which make the wind power curtailment remain significant, resulting in low wind energy utilization. If these problems are not properly solved, the security of operations cannot be well maintained, and the reliability and cost-effectiveness of the power system cannot be optimized.

As an effective means to realize the time-sequence shift of power and energy, an energy storage system can enhance the peak regulation capability of the power system, to achieve peak load shifting [6] and store surplus wind power [7]. For a storage device with fast response, it can also participate in FFR, PFR, and SFR [8] through charging and discharging, to improve the frequency regulation capability of the power system and improve the frequency security and reliability. Among many energy storage devices, a modern battery energy storage station (BESS) is a type of storage with fast response [9,10], which therefore can alleviate the above-mentioned FCASs problems [11,12]. Technological maturity and reduced costs of batteries have welcomed its wide application in power systems. In the context of the increasingly prominent FCASs problem, batteries systems are considered a promising means of energy storage. In particular, an LS-BESS with a comparable scale of a typical generation unit, can play a better role as the proportion of non-dispatchable renewable energy resources keeps increasing in the power grid, leading to increasingly less active power regulation

* Corresponding author.
E-mail address: wdli@dlut.edu.cn (W. Li).

https://doi.org/10.1016/j.rser.2023.113963
Received 23 March 2022; Received in revised form 28 August 2023; Accepted 18 October 2023
Available online 7 November 2023

Nomenclature

C_{op}, C_{re}, C_{risk} Operation, reserve, and risk costs of the system in the whole dispatch day ($)
$C^{b}_{g,i,t}$, $C^{e}_{g,i,t}$ Startup and shutdown costs of generation unit i in period t ($)
$C^{ge}_{g,i,t}$ Production cost of generation unit i in period t ($)
$C^{\mathrm{DPR}}_{g,i,t}$ Deep peak regulation cost of generation unit i in period t ($)
$c^{\mathrm{FFR}}_{\mathrm{B}}$, $c^{\mathrm{PFR}}_{\mathrm{B}}$, $c^{\mathrm{SFR}}_{\mathrm{B}}$ Unit compensation costs of participating in fast frequency regulation (FFR), primary frequency response (PFR), and secondary frequency regulation (SFR) for a LS-BESS ($/MWh)
c^{SFR}_{g} Unit compensation cost of participating in SFR for a generation unit ($/MWh)
$R^{\mathrm{load}}_{1,t}$ The under-frequency load shedding (UFLS) loss in period t ($)
c^{load}, c_{W} Unit loss costs of load curtailment and wind energy curtailment ($/MWh)
$u_{i,t}$ Binary variable: "1" if generation unit i is ON in period t, and "0" otherwise
v_t Binary variable: "1" if LS-BESS is discharging in period t, and "0" otherwise
$P_{g,i,t}$ Power output of generation unit i in period t (MW)
$P^{\max}_{g,i}$, $P^{\min}_{g,i}$ Maximum and minimum power output of generation unit i (MW)
$V^{+}_{g,i}$, $V^{-}_{g,i}$ Ramp-up and ramp-down limits of generation unit i (MW per time step)
$P^{\mathrm{ch}}_{\mathrm{B},t}$, $P^{\mathrm{dis}}_{\mathrm{B},t}$ Charging and discharging power of LS-BESS in period t (MW)
$P^{\max}_{\mathrm{B}}$, $E^{\mathrm{rated}}_{\mathrm{B}}$ Rated power and energy capacities of LS-BESS (MW and MWh)
$E_{\mathrm{B},t}$ Energy capacity of LS-BESS in period t (MWh)
η_{ch}, η_{dis} Charging and discharging rates of LS-BESS
$\mathrm{SoC}^{\mathrm{ini}}_{\mathrm{B}}$ State of charge (SoC) of LS-BESS in the initial period of the dispatch day
$\Delta P_{\mathrm{L},t}$ Power shortage or deficiency within period t (MW)
$H_{\mathrm{S},t}$ Equivalent inertia time constant of the system in period t (s)
$K^{\mathrm{PFR}}_{g,i}$ Droop coefficient of generation unit i (MW/Hz)
$K^{\mathrm{FFR}}_{\mathrm{B},t}$ Virtual regulation coefficient of LS-BESS participating in FFR in period t (MWs/Hz)
$K^{\mathrm{PFR}}_{\mathrm{B},t}$ Virtual droop coefficient of LS-BESS in period t (MW/Hz)
HF_t Proportion of the high-frequency components of frequency fluctuations in period t
γ Minimum spinning reserve rate required by the system
$f^{\min}$ Pre-specified frequency limit to trigger the UFLS relay (Hz)

resources. Having the combined advantages of power-type and energy-type storage components, a LS-BESS can provide peak regulation with energy demand and SFR service for both power and energy in normal operations, and can be used as an emergency regulation resource for FFR and PFR after a large step disturbance to ensure frequency stability. For a LS-BESS to effectively participate in multi-regulations, optimal day-ahead dispatch for a power system with the LS-BESS and wind energy is required. The main goal of the day-ahead dispatch is to determine the next-day generation units' scheduling and spinning reserves needed, so that the multi-regulations can be satisfied, and frequency stability can be guaranteed by the orchestrated energy resources. This has motivated this research.

Currently, some studies have considered a BESS as a means of providing FCAS for a power system, and we have briefly summarized them. From the analytical perspective of this study, BESSs can be classified into two categories: direct and non-direct dispatch BESSs. Non-direct-dispatch of BESSs means that the BESSs cannot be directly dispatched by bulk power grid operators due to their small capacities, and their participation in one or more types of FCASs is generally based on some response incentive mechanisms [9,13,14] or aggregated in virtual power plants [15,16] to participate in power system ancillary services. The operational strategies for this type of BESSs are developed by the BESS control center or the virtual power plant control center from their own perspectives.

In other words, the operation and control of the above-mentioned BESSs are not directly dispatched by bulk power grid operators. They are either autonomously adjusted according to the frequency control signal or coordinated by the aggregators or collaborative power generation operators. Therefore, the operation strategies of participating in FCASs are not applicable to directly dispatched BESSs. While some studies involve BESSs that are directly dispatched by grid operators, they focus on determining the optimal bidding strategies for BESSs in multi-type FCASs participation. For example, studies in Refs. [17–19] proposed a control strategy and optimal clearing scheduling method of a BESS to participate in the PFR and energy markets to realize high profitability under the day-ahead electricity market mechanism. These studies reflect BESS-centric decision-making, which is not a holistic method for bulk grid operators' system-wide decisions.

For a BESS that can be directly dispatched by bulk power grid operators, its unexpected actions outside the dispatch expectation may have a massive impact on the power grid, due to its large power and energy capacity. Therefore, a LS-BESS should be managed through the central power dispatch from a holistic perspective of power grid operations. However, there are only a few research attempts on how to fully utilize its advantage and complement a LS-BESS and other sources. This is an especially important research direction to realize a suitable dispatch scheme of grid-scale LS-BESS-incorporated power systems. If a LS-BESS only provides a single service, it is not conducive to realizing its full regulation potential and short-term return on investment. Therefore, a LS-BESS should participate in multi-regulation services in the power system to better serve the grid operations. Studies in Refs. [17–21] consider one or two types of regulations, but have not involved the coordination of various FCASs at the full timescale in daily operations, or considered the potential operational risk of the power grid. Therefore, it is hard to achieve better coordination among secure, reliable, and economic power grid operations.

For day-ahead dispatch strategies of wind-energy-integrated power grids with a LS-BESS, it is necessary to consider the uncertainty of wind power output [22], which requires an appropriate stochastic optimization approach. The chance-constrained programming reported in Ref. [23] accepts optimization decisions that do not meet the constraints, but within a certain range. This may lead to the day-ahead optimization results unsuitable for the grid operations in the dispatch day. The scenario-based stochastic programming model in Ref. [24] can obtain a dispatch scheme that considers the actual characteristics of each typical scenario, which is generally applicable to the situations where the actual probability distribution of the uncertainties can be effectively obtained. Under the condition of unknown probability, the RO method [25,26] shows great advantages, and the obtained optimization strategy is effective for any scenario in the uncertainty set. However, the decisions resulting from the standard RO are usually overly conservative, leading to limited profitability. The RO approach based on the budget uncertainty set can improve this problem [27,28], and it is favored by some studies. The uncertainty set is generated by

using the offsets of wind power output uncertainty to characterize the uncertainty degree.

Considering operational risks in power dispatch can realize fine management of reserve spaces. To ensure secure grid operations [10,29], reserve space is allocated based on the worst disturbances under a given prediction failure set, which realizes reliable system operations. However, this implies significant excessive reserve cost for the system. Many unnecessary reserve spaces will be allocated to deal with the low-probability extreme distributions, which is not conducive to the power system economy in long-term operations. For this problem, the studies in Refs. [30,31] have adopted the risk analysis method by using value-at-risk (VaR) as a metric to achieve economic reserve, which consider the maximum loss of uncertain disturbances to the system at a given confidence level. This method is equivalent to truncating the whole operation situations, which makes the method difficult to cope with the risks beyond the confidence level. To address this drawback, the conditional VaR (i.e., CVaR) theory attracts much attention. CVaR focuses on characterizing the loss of extreme situations outside the confidence level. Taking CVaR as a metric, a risk dispatch model of the power system considering uncertain factors is established in Refs. [32,33], to replace the conventional scheduling framework. However, there has been no reported work on how to effectively measure the power system risk after a LS-BESS is considered in grid operations. This can realize the coordination among the three types of FCASs with limited regulation resources.

In summary, current dispatch schemes fall short of optimizing LS-BESS utilization in grid dispatch for comprehensive source coordination across various FCASs. To address this research gap, this study introduces a day-ahead dispatch model that integrates an LS-BESS and conventional generation units within wind-energy-integrated power grids. This model is designed to offer multi-regulation services while considering operational risks. The main contribution of this study can be summarized as follows.

- For bulk power grid operators, collaborative operation strategies are proposed from a holistic perspective of power system operations for the joint participation of a directly dispatchable LS-BESS and generation units in full-timescale FCASs during daily operations.
- An advanced day-ahead risk-analysis dispatch model is formulated. It accounts for power system uncertainties across various timescales of power disturbances and coordinates three types of FCASs. This model achieves optimal coordination among power grid security, operational quality, and economic efficiency.
- To better tackle uncertainty in step disturbances, non-step disturbances, and wind power output over a large timescale, the proposed dispatch model utilizes scenario-based stochastic programming with expected probability, and the RO approach based on a budget uncertainty set. The aim of this model is to enhance the model's practicality. To mitigate risks from unpredictable wind power fluctuations, the model employs an interval acceptance strategy for wind power, offering improved operational flexibility. Additionally, to effectively quantify potential losses arising from insufficient FCAS regulations, the study adopts the CVaR theory. This enables the consideration of both the maximum expected loss under normal conditions and the tail risk during extreme scenarios.

It should be noted that the LS-BESS involved in this study is conceptualized as a BESS whose power capacity and energy capacity have reached scales that can be directly dispatched by the bulk power grid operators. This operation and control are managed by dispatch instructions, which can solve the problem of insufficient frequency regulation capacity of the power systems. The rest of this work is organized as follows. Section 2 introduces the participation of LS-BESS in multi-regulation services in a power system. Section 3 establishes the proposed day-ahead dispatch model. Section 4 presents the proposed risk analysis method. Section 5 provides the solving method and numerical study. Finally, this study concludes in Section 6.

2. Coordination of LS-BESS participating in FCASs

Power systems are impacted by diverse types of power disturbances in daily operation, which needs to be regulated by FCASs to ensure secure, high-quality, and economic power supply. Disturbances can be divided into step and non-step disturbances within a certain period, and net load changes over a large timescale. In this section, the characteristics of three types of FCASs are analyzed to clarify their relations and dispatch requirements from a system perspective.

2.1. Three types of FCASs

1) First type, responding to step disturbances: Sudden changes in the grid, such as load increase and line disconnection, bring step disturbances to the system at a short timescale of a few or tens of milliseconds. After a such disturbance occurs, power-type services IFR and PFR supply a large amount of power to support power generation and thus slow down the frequency drop [2]. IFR comes from the kinetic energy of generation units' rotors, which starts to respond when the system is disturbed, and can last for 0–5s [34]. When the frequency drops below a dead band f^{db} set by generation units, units start providing PFR, which can remain 5–60s.

The large and small step disturbances appearing in the system are random. Although the probability of a large disturbance is low, this scenario should still be considered in day-ahead scheduling to minimize operational risks during the next day. Two dynamic characteristic indexes should be considered for the transient low-frequency process caused by step disturbances [1,2], the initial rate of change of frequency $RoCoF^{0^+}$ and the frequency nadir point f^{nadir}. The risk of this type of disturbance comes from the UFLS due to insufficient system inertia and PFR reserve, which has a significant impact on secure operations.

2) Second type, responding to non-step disturbances: Under normal operations, the actual net load (the difference between wind power and load) within each period would inevitably change, which causes minute-level non-step disturbances to the system. Different from the instantaneous step disturbances, net load fluctuations are relatively slow and last for a long time. They must be regulated to avoid frequency swings, leading to undermined power quality or reliability. The fluctuations include high-frequency components with small amplitudes and rapid changes, and low-frequency devices with relatively large yet slow changes [35]. Therefore, the service combined power-type and energy-type SFR that can last for 30s–15mins responds to this type of disturbances. So, it is necessary for SFR resources to reserve some upper and lower SFR spaces in the day-ahead scheduling stage.

In the day-ahead data, load forecasting is usually more accurate than wind energy forecasting. Authors in Refs. [36,37] present that the load forecasting error is ±3–5%, while the error of wind power prediction can reach ±10–21%. Therefore, to ensure reliable daily operation, a ±5% load forecasting error is adopted in this study. The fluctuation degree of wind power is further characterized in the following sections. The risk comes from wind curtailment loss caused by insufficient lower SFR reserve bound when the highest fluctuations of wind power occur, and load shedding loss by insufficient upper SFR bound for the lowest wind fluctuations.

3) Third type, responding to net load changes: Net load changes need to be tracked by adjusting the number of startup and shutdown of generation units, as well as the power output of generation units, to realize power balance. Therefore, it is necessary to formulate the unit commitment and output benchmark of each generation unit in the day-ahead dispatch [29]. Within a dispatch day, the timescale of net load changes is large, which leads to high energy requirement for regulation resources to have sufficient capacities to respond to the changes. So, the energy-type service of peak regulation is the main means of responding

to this change. After the wind power as a negative load is connected to the grid, the original load curve is widened, and zenith-nadir difference of net load is increased. In the case of limited system downward peak shaving capacity, when the wind power is high, whether to cut down the wind power or put generation units into the deep peak regulation states [38] significantly increases system operation cost. From a day-ahead perspective, the actual wind power in each period is uncertain, but its output range can be determined. Moreover, its forecasting error within the period can be ignored compared with the amount of required peak regulation capacity. Thus, the large-term net load changes have strong certainty compared to the step and non-step disturbances.

2.2. Participation of LS-BESS

A LS-BESS can realize fast and high-power regulation and has sufficient energy, which can act as a power-type regulation resource, achieve energy-type control, and participate in FCASs as a power-energy interactive system. As such a LS-BESS can realize FFR [39] and PFR through virtual generation unit's IFR and droop control. This can compensate for insufficient regulation capacities of generation units, to participate in the first type of FCAS to enhance the system's resilience under large step disturbances. For the second type of FCAS, to collectively utilize complementary advantages of resources, a LS-BESS can suppress high-frequency components during net load fluctuations, and low-frequency components can be managed by SFR generation units. A LS-BESS has bidirectional regulation feature, which can be charged when energy on the supply side is sufficient to increase the peak regulation capability of the system.

As discussed in Section 2.1, three types of FCASs have different timescales and uncertainty degrees, but with overlaps on power and energy types of regulation resources. Therefore, operators can comprehensively optimize the day-ahead reverse of each regulation resource through different timescale coordination, the complementarity between power and energy demand types, and the risk analyses among different services' uncertainties. Different from the strategy which tries to ensure the secure and stable operations of the system under a given prediction failure set [25], this study allows insufficient regulation of each service to bring loss to the system. Like in real-world operation, idea of risk analysis means that the security of the system under all disturbances is not guaranteed, and the trade-off between the spinning reserve and the potential loss is determined by the optimization strategy based on the CVaR theory.

The large timescale changes of wind power are dealt with the third type of FCAS, and short timescale fluctuations are managed by the second type. Therefore, the day-ahead dispatch strategy includes the reserved upper and lower SFR bounds to cope with wind power fluctuations, which makes the acceptance value $P_{W,t}$ of wind power in each period replaced by an interval $\left[\check{P}_{W,t}, \hat{P}_{W,t}\right]$. The RO approach based on the budget uncertainty set can control the offset of the uncertainty of the actual wind power $P^{act}_{W,t}$, which can avoid the over-conservatism of the standard RO. It can be employed in day-ahead dispatch to make more robust and realistic decisions. Comprehensive coordination among multi-regulations is essentially a nonlinear programming problem. The optimal strategies are obtained by solving the mathematical model with the goal of minimizing the total operation cost C^{DA} of the system over the dispatch day. This achieves better coordination of three types of FCASs, and further contribute to a secure, reliable, and economic power supply. Fig. 1 is an overall diagram to illustrate the proposed day-ahead dispatch.

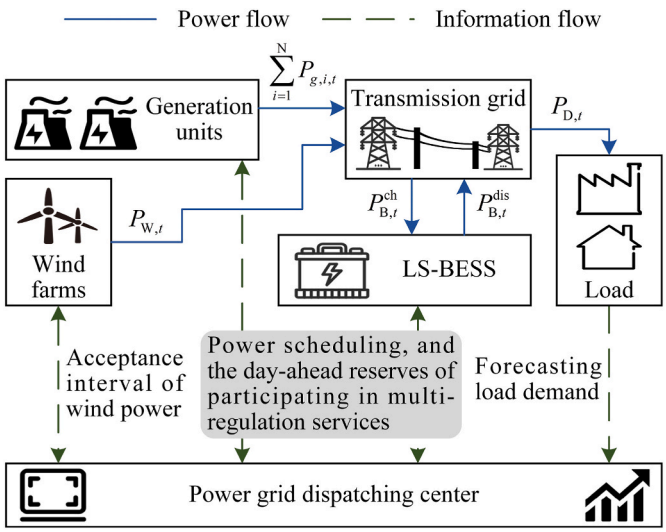

Fig. 1. The operation framework of the day-ahead dispatch.

3. Day-ahead dispatch model

3.1. Objective function

A scheduling day is divided into 96 time steps for day-ahead dispatch, and each step Δt is 15 minutes. The optimization objective is formulated as

$$\text{minimize} \quad C^{DA} = C_{op} + C_{re} + C_{risk} \tag{1}$$

1) C_{op}: This term contains the operation costs $C_{B,op}$ and $C_{g,op}$ of a LS-BESS and generation units, i.e.,

$$C_{op} = C_{B,op} + C_{g,op} \tag{2}$$

where

$$C_{B,op} = c_{B,op} \sum_{t=1}^{96} \left(P^{ch}_{B,t} + P^{dis}_{B,t}\right) \Delta t \tag{3a}$$

$$C_{g,op} = \sum_{i=1}^{N} \sum_{t=1}^{96} \left(C^{b}_{g,i,t} + C^{e}_{g,i,t} + C^{ge}_{g,i,t} + C^{DPR}_{g,i,t}\right) \tag{3b}$$

$$C^{b}_{g,i,t} = c^{on}_{g,i} \left(1 - u_{i,t-1}\right) u_{i,t} \tag{3c}$$

$$C^{e}_{g,i,t} = c^{off}_{g,i} u_{i,t-1} \left(1 - u_{i,t}\right) \tag{3d}$$

$$C^{ge}_{g,i,t} = \left(a_i P^2_{g,i,t} + b_i P_{g,i,t} + c_i u_{i,t}\right) \Delta t \tag{3e}$$

$$C^{DPR}_{g,i,t} = \begin{cases} c^{DPR1}_{g} \left(P^{DPR1}_{g,i} - P_{g,i,t}\right) \Delta t, \text{only if } P^{DPR2}_{g,i} < P_{g,i,t} \le P^{DPR1}_{g,i} \\ c^{DPR1}_{g} \left(P^{DPR1}_{g,i} - P^{DPR2}_{g,i}\right) \Delta t + c^{DPR2}_{g} \left(P^{DPR2}_{g,i} - P_{g,i,t}\right) \Delta t, \text{only if } P_{g,i,t} \le P^{DPR2}_{g,i} \end{cases} \tag{3f}$$

In (3a), $c_{B,op}$ is the unit power operation cost of a LS-BESS. In (3b), term N is the total number of generation units in the system, and the startup, shutdown, and production costs are described by (3c), (3d), and (3e). In (3f), $P_{g,i}^{DPR1}$ and $P_{g,i}^{DPR2}$ are the critical values of unit i stepping into the first and second gears of deep peak regulation, and c_g^{DPR1} and c_g^{DPR2} are the unit electricity costs in each gear. According to the "Operation rules of northeast electric power ancillary service market" in Ref. [40], the deep peak regulation of a generation unit is traded in a "ladder" manner with two gears. The compensation benchmark of the first gear of deep peak regulation is that the load rate of the unit is within the range of (40%, 50%], and the load rate of the second gear of deep peak regulation is less than or equal to 40%. So, we have $P_{g,i}^{DPR1} = 50\%P_{g,i}^{max}$, and $P_{g,i}^{DPR2} = 40\%P_{g,i}^{max}$.

2) C_{re}: The LS-BESS reserves $P_{B,t}^{FFR}$ and $P_{B,t}^{PFR}$ to participate in FFR and PFR in period t. In addition, the LS-BESS and generation unit j reserve the upper SFR $P_{B,t}^{SFR,up}$ and $P_{g,j,t}^{SFR,up}$, and lower $P_{B,t}^{SFR,down}$ and $P_{g,j,t}^{SFR,down}$, respectively. Parameter C_{re} is calculated as

$$C_{re} = C_B^{FFR} + C_B^{PFR} + C_B^{SFR} + C_g^{SFR} \tag{4}$$

where

$$C_B^{FFR} = c_B^{FFR}\sum_{t=1}^{96}\left(P_{B,t}^{FFR}\Delta t\right) \tag{5a}$$

$$C_B^{PFR} = c_B^{PFR}\sum_{t=1}^{96}\left(P_{B,t}^{PFR}\Delta t\right) \tag{5b}$$

$$C_B^{SFR} = c_B^{SFR}\sum_{t=1}^{96}\left(\left(P_{B,t}^{SFR,up} + P_{B,t}^{SFR,down}\right)\Delta t\right) \tag{5c}$$

$$C_g^{SFR} = c_g^{SFR}\sum_{j=1}^{M}\sum_{t=1}^{96}\left(\left(P_{g,j,t}^{SFR,up} + P_{g,j,t}^{SFR,down}\right)\Delta t\right) \tag{5d}$$

For a generation unit, participating in IFR and PFR is its inherent attribute and obligatory action [1], and therefore units are not compensated for providing IFR and PFR in our algorithm. But a LS-BESS needs to be compensated for its participation in the regulations, as described in (5a)–(5c). In (5d), term M is the total number of SFR generation units in the system.

3) C_{risk}: Considering the regulation violation losses R_1, R_2, and R_3 of the system caused by the insufficient regulation capacity for the first, second, and third types of FCASs, the risk cost C_{risk} is defined as

$$C_{risk} = \xi_1 R_1 + \xi_2 R_2 + \xi_3 R_3 \tag{6}$$

In (6), R_1 is the UFLS loss of the system caused by step disturbances, and R_2 consists of $R_{2,t}^{wind}$ and $R_{2,t}^{load}$, i.e., wind power curtailment loss and loss associated with load shedding under the wind power fluctuations $\Delta P_{W,t}^{act}$ in period t. Term R_3 is used to represent the total of wind power curtailment costs over all time periods on the dispatch day. In real-world power system operations, with limited regulation resources, different types of frequency control services have different importances. In this study, risk aversion coefficients ξ_1, ξ_2, and ξ_3 are introduced to represent the weights of the first, second, and third types of FCASs, to reflect the risk preference degree of a decision maker. If in an extreme case ξ_x=0, the operator weighs the risk associated with the x-th type of FCAS negligible. The larger value of ξ, the more conservative operator is, and the greater operation and reserve costs required to avoid potential losses. In general, the dispatch takes more initiative to avoid the loss of load shedding caused by step disturbances, therefore this work sets $\xi_1 > \xi_2 > \xi_3$. Calculations of R_1, R_2, and R_3 are provided in Section 4.

3.2. Constraints of the proposed day-ahead dispatch model

A range of constraints are enforced for generators, as in (7a)–(10f), and the power network, as in (11)–(20d). Some transmission lines may be overloaded for a period after an accident, and the overload time is usually longer than the frequency dynamic response. Therefore, transmission constraints are usually excluded in dispatch research when considering the participation of the BESS in active power regulation services [10].

1) Constraints of generation units:

$$u_{i,t} - u_{i,t-1} - u_{i,\varsigma} \le 0, \quad t \le \varsigma \le T_i^{on} + t - 1 \tag{7a}$$

$$u_{i,t-1} - u_{i,t} + u_{i,\vartheta} \le 1, \quad t \le \vartheta \le T_i^{off} + t - 1 \tag{7b}$$

$$u_{i,t}P_{g,i}^{min} \le P_{g,i,t} \le u_{i,t}P_{g,i}^{max} \tag{7c}$$

$$P_{g,i,t+1} - P_{g,i,t} \le V_{g,i}^{+}u_{i,t} + P_{g,i}^{max}\left(1 - u_{i,t}\right) \tag{7d}$$

$$P_{g,i,t} - P_{g,i,t+1} \le V_{g,i}^{-}u_{i,t+1} + P_{g,i}^{max}\left(1 - u_{i,t+1}\right) \tag{7e}$$

$$P_{g,i,t} + P_{g,i,t}^{PFR} \le u_{i,t}P_{g,i}^{max} \tag{7f}$$

$$P_{g,i,t}^{PFR} = u_{i,t}K_{g,i}^{PFR}\left(\Delta f^{max} - f^{db}\right) \tag{7g}$$

$$P_{g,j,t} - P_{g,j,t}^{SFR,down} \ge u_{j,t}P_{g,j}^{min} \tag{7h}$$

$$P_{g,j,t} + P_{g,j,t}^{PFR} + P_{g,j,t}^{SFR,up} \le u_{j,t}P_{g,j}^{max} \tag{7i}$$

In (7a) and (7b), T_i^{on} and T_i^{off} are the minimum ON and OFF time of generation unit i. The production and ramping limits are expressed in (7c)–(7e). Constraint (7f) shows the limit for PFR reserve, and (7g) describes the power of PFR where Δf^{max} is the maximum frequency deviation for the droop relation. Constraints (7h) and (7i) show the limits associated with the SFR reserve. Considering that the online generation units must participate in PFR, but not all units can undertake SFR. Therefore, all generation units need to meet constraint (7f). For SFR units, constraints (7f), (7h), and (7i) are also enforced.

2) Constraints of the LS-BESS:

$$0 \le P_{B,t}^{ch} \le P_B^{max}(1 - v_t) \tag{8a}$$

$$0 \le P_{B,t}^{dis} \le P_B^{max}v_t \tag{8b}$$

$$\Delta E_{B,t} = P_{B,t}^{dis}\Big/\eta_{dis}\Delta t - P_{B,t}^{ch}\eta_{ch}\Delta t \tag{8c}$$

$$\Delta E_{B,t}^{FFR} = P_{B,t}^{FFR}\Big/\eta_{dis}\Delta t_1 \tag{8d}$$

$$\Delta E_{B,t}^{PFR} = P_{B,t}^{PFR}\Big/\eta_{dis}\Delta t_2 \tag{8e}$$

$$\Delta E_{B,t}^{SFR} = P_{B,t}^{SFR,up}\Big/\eta_{dis}\Delta t - P_{B,t}^{SFR,down}\eta_{ch}\Delta t \tag{8f}$$

$$E_{B,t+1} = E_{B,t} - \left(\Delta E_{B,t} + \Delta E_{B,t}^{FFR} + \Delta E_{B,t}^{PFR} + \Delta E_{B,t}^{SFR}\right) \tag{8g}$$

$$E_B^{rated}SoC_B^{min} \le E_{B,t} \le E_B^{rated}SoC_B^{max} \tag{8h}$$

$$E_{B,1} = E_{B,97} = SoC_B^{ini}E_B^{rated} \tag{8i}$$

$$0 \le P_{B,t}^{FFR} + P_{B,t}^{PFR} + P_{B,t}^{SFR,up} \le P_B^{max} - P_{B,t}^{dis} + P_{B,t}^{ch} \tag{8j}$$

$$0 \le P_{B,t}^{SFR,down} \le P_B^{max} + P_{B,t}^{dis} - P_{B,t}^{ch} \tag{8k}$$

The charging and discharging power limits of the LS-BESS are described in (8a) and (8b). Constraints (8c)–(8f) show the relationship of power and energy. Constraints (8d)–(8e) represent the energy spaces reserved by a LS-BESS to participate in the FFR and PFR services, which are set for the system subjected to step disturbances. Terms Δt_1 and Δt_2 are 5s and 60s, respectively. After a step disturbance occurs, the time-scale of frequency drop is in seconds. Therefore, the timescale of a LS-BESS response to the first type of FCAS is also in seconds or tens of seconds, and its reserved energy space should be calculated according to the response time of FFR and PFR. Grid operators need to make a LS-BESS reserve the spaces required for participating in FFR and PFR in the entire dispatch time. The time-coupled constraint is represented by (8g). Constraint (8h) limits the upper and lower thresholds of the operation capacity of the LS-BESS, and $\mathrm{SoC}_{\mathrm{B}}^{\max}$ and $\mathrm{SoC}_{\mathrm{B}}^{\min}$ are the maximum and minimum SoC. The daily operation cycle is written as (8i), and the upper and lower reserved spaces are considered in (8j) and (8k).

3) Constraints of wind power: $P_{\mathrm{W},t}$ satisfies

$$0 \le P_{\mathrm{W},t} \le P_{\mathrm{W},t}^{\mathrm{act}} \tag{9}$$

where

$$P_{\mathrm{W},t}^{\mathrm{act}} \in \left[P_{\mathrm{W},t}^{\min}, P_{\mathrm{W},t}^{\max}\right] \tag{10a}$$

$$P_{\mathrm{W},t}^{\mathrm{act}} = P_{\mathrm{W},t}^{\mathrm{pre}} + P_{\mathrm{W},t}^{\mathrm{unc}} \tag{10b}$$

$$P_{\mathrm{W},t}^{\mathrm{pre}} = \left(P_{\mathrm{W},t}^{\max} + P_{\mathrm{W},t}^{\min}\right) \Big/ 2 \tag{10c}$$

$$P_{\mathrm{W},t}^{\mathrm{unc}} = z_{\mathrm{W},t}\left(P_{\mathrm{W},t}^{\max} - P_{\mathrm{W},t}^{\min}\right) \Big/ 2 \tag{10d}$$

$$\mathbf{Z}_{\mathrm{W}} = \left(z_{\mathrm{W},1}, z_{\mathrm{W},2}, \ldots, z_{\mathrm{W},96}\right)^{\mathrm{T}} \tag{10e}$$

$$\|\mathbf{Z}_{\mathrm{W}}\|_1 \le \Gamma_{\mathrm{W}} \tag{10f}$$

In (10), the uncertainty of wind power output on the dispatch day is characterized by the RO approach based on the budget uncertainty set, where $P_{\mathrm{W},t}^{\mathrm{act}}$ is recorded as the superposition between the forecasted value and the uncertain factor. Term $z_{\mathrm{W},t}$ is the offset of the uncertainty factor, and Γ_{W} is the budgeted value.

4) Constraint of the power balance: Active power of the system must satisfy supply and demand balance, i.e.,

$$\sum_{i=1}^{\mathrm{N}} P_{g,i,t} + \left(P_{\mathrm{B},t}^{\mathrm{dis}} - P_{\mathrm{B},t}^{\mathrm{ch}}\right) + P_{\mathrm{W},t} = P_{\mathrm{D},t} \tag{11}$$

where $P_{\mathrm{D},t}$ is the system load demand in period t. This constraint is designed for net load changes.

5) Constraint of spinning reserve: The total reserve of generators should guarantee the minimum spinning reserve requirement of the system, and therefore, we have

$$\sum_{i=1}^{\mathrm{N}} u_{i,t}\left(P_{g,i}^{\max} - P_{g,i,t}\right) + \left(P_{\mathrm{B}}^{\max} - P_{\mathrm{B},t}^{\mathrm{dis}} + P_{\mathrm{B},t}^{\mathrm{ch}}\right) \ge \gamma P_{\mathrm{D},t} \tag{12}$$

6) Supporting step disturbances: After describing the dynamic characteristics of the system frequency by the first-order swing equation, $RoCoF^{0^+}$ is determined as follows [19],

$$RoCoF_t^{0^+} = \frac{\Delta P_{\mathrm{L},t} f_0}{2 H_{\mathrm{S},t} P_b} \tag{13}$$

and it should be constrained within a certain range:

$$RoCoF_t^{0^+} \le RoCoF^{\max} \tag{14}$$

where $RoCoF^{\max}$ is the maximum value of the $RoCoF^{0^+}$.

In (13), term f_0 is the nominal system frequency, and P_b is the baseline capacity of the system, which is the sum of power capacities of all generators that can participate in step disturbances regulation. In addition, $H_{\mathrm{S},t}$ is computed as [1]

$$H_{\mathrm{S},t} = \left(\sum_{i=1}^{\mathrm{N}}\left(H_i P_{g,i}^{\max} u_{i,t}\right) + H_{\mathrm{B},t} P_{\mathrm{B}}^{\max}\right) \Big/ P_b \tag{15}$$

where H_i is the inertia time constant of generation unit i, and $H_{\mathrm{B},t}$ is the virtual inertia time constant in period t of the LS-BESS.

Conservatively, $P_{\mathrm{B},t}^{\mathrm{FFR}}$ is reserved with the limit of $RoCoF^{\max}$, and

$$P_{\mathrm{B},t}^{\mathrm{FFR}} = K_{\mathrm{B},t}^{\mathrm{FFR}} RoCoF^{\max} \tag{16}$$

where

$$K_{\mathrm{B},t}^{\mathrm{FFR}} = 2\frac{H_{\mathrm{B},t} P_{\mathrm{B}}^{\max}}{f_0} \tag{17}$$

The total amount $P_{\mathrm{S},t}^{\mathrm{PFR}}$ of the reserved PFR in the system is provided by generation units and the LS-BESS, which is written as

$$P_{\mathrm{S},t}^{\mathrm{PFR}} = \sum_{i=1}^{\mathrm{N}} P_{g,i,t}^{\mathrm{PFR}} + P_{\mathrm{B},t}^{\mathrm{PFR}} \tag{18}$$

Variable $P_{\mathrm{B},t}^{\mathrm{PFR}}$ is optimized in the day-ahead dispatch, so that the LS-BESS has the space to respond to frequency deviation through real-time virtual droop control. There is a maximum linear regulation frequency $\Delta f^{\max}$ in the process of generation units participating in PFR, i.e., the regulation limit (as in (7g)). When the frequency difference exceeds $\Delta f^{\max}$, generation units cannot increase their outputs further. In this case, the LS-BESS can be dispatched to make up for the capacity shortage. To give full consideration to the inherent regulation ability of generation units and ensure that the LS-BESS can be quickly dispatched when the capacity of units is insufficient, this study sets the frequency dead band of PFR of the LS-BESS to $\Delta f^{\max}$. Power $P_{\mathrm{B},t}^{\mathrm{PFR}}$ can be determined by the following linear virtual droop relation,

$$P_{\mathrm{B},t}^{\mathrm{PFR}} = K_{\mathrm{B},t}^{\mathrm{PFR}}\left(f_0 - f^{\min} - \Delta f^{\max}\right) \tag{19}$$

7) Suppressing non-step disturbances: Constraints include

$$\sum_{j=1}^{\mathrm{M}} P_{g,j,t}^{\mathrm{SFR,up}} + P_{\mathrm{B},t}^{\mathrm{SFR,up}} = P_{\mathrm{W},t} - \breve{P}_{\mathrm{W},t} + 5\%P_{\mathrm{D},t} \tag{20a}$$

$$\sum_{j=1}^{\mathrm{M}} P_{g,j,t}^{\mathrm{SFR,down}} + P_{\mathrm{B},t}^{\mathrm{SFR,down}} = \widehat{P}_{\mathrm{W},t} - P_{\mathrm{W},t} + 5\%P_{\mathrm{D},t} \tag{20b}$$

$$P_{\mathrm{B},t}^{\mathrm{SFR,up}} = \mathrm{HF}_t\left(P_{\mathrm{W},t} - \breve{P}_{\mathrm{W},t} + 5\%P_{\mathrm{D},t}\right) \tag{20c}$$

$$P_{\mathrm{B},t}^{\mathrm{SFR,down}} = \mathrm{HF}_t\left(\widehat{P}_{\mathrm{W},t} - P_{\mathrm{W},t} + 5\%P_{\mathrm{D},t}\right) \tag{20d}$$

Constraints (20a) and (20b) represent the upper and lower reserved spaces for regulation capacity demand, and (20c) and (20d) calculate the regulation rates.

4. Risk analysis and quantification

In this section, the risk analysis method is detailed and terms R_1, R_2, and R_3 that appeared in (6) are calculated.

4.1. Risk measurement method

Risk analysis is an effective way for risk management, which aims to meticulously measure and reduce losses caused by any operation risks

[41]. Risk measurement is usually realized mainly through the minimal variance and VaR and CVaR theories proposed in Refs. [41,42]. The latter option not only considers the maximum expected loss under normal operations, but also covers the probability-weighted average losses under extreme tail conditions beyond the confidence level. As such the CVaR is adopted in this study, which is adapted to weigh the relationship between reserved spaces and corresponding risk losses.

Let x be the decision variable, u be the random variable, and $f(u)$ be the probability density function (PDF) of u. For a fixed x, the losses caused by the change of u constitute the function $h(x, u)$, whose upper boundary is α. The probability (cumulative distribution function) of $h(x, u)\leq\alpha$ is written as

$$\Psi(x,\alpha)=\int_{h(x,u)\leq\alpha} f(u)du \tag{21}$$

The minimum value of α satisfies the condition $\Psi(x,\alpha)\geq\beta$ for a given confidence level β is the VaR, i.e.,

$$\mathrm{VaR}=\alpha_\beta(x)=\min\{\alpha|\Psi(x,\alpha)\geq\beta\} \tag{22}$$

where β satisfies $0<\beta<1$. In practical terms, this means that with probability 1-β, the decision makers allow the loss to be at a certain risk level.

The VaR method limits the boundary of loss to $\alpha_\beta(x)$, while CVaR focuses on the case when $h(x, u)\geq\alpha_\beta(x)$. Calculating the conditional mean value after the loss exceeds VaR, we have

$$\mathrm{CVaR}=(1-\beta)^{-1}\int_{h(x,u)\geq\alpha_\beta(x)} h(x,u)f(u)du \tag{23}$$

Therefore, the risk loss obtained by considering the CVaR method is written as

$$F_\beta(x,\alpha)=\alpha+(1-\beta)^{-1}\int[h(x,u)-\alpha]^+f(u)du \tag{24}$$

where

$$[h(x,u)-\alpha]^+=\max\{h(x,u)-\alpha,0\} \tag{25}$$

If $f(u)$ cannot be written in an analytical expression, the random variable u can be discretized into m intervals, i.e., u_1, u_2, …, u_m. In this case, the risk loss is recorded as:

$$F_\beta(x,\alpha)=\alpha+(1-\beta)^{-1}m^{-1}\sum_{k=1}^{m}[h(x,u_k)-\alpha]^+ \tag{26}$$

It should be noted that all parameters defined in this section are only used for the theories in Section 4.1.

4.2. Regulation violation penalties calculation

1) R_1: According to the results of situational awareness of system operations on the second day, the possible step disturbance values within period t are sorted in ascending order. This forms a set with Q_t elements. The occurrence probability of each disturbance is $pr(\Delta P_{\mathrm{L},t}^{q_t})$, where $q_t=1,\ \ldots,\ \mathrm{Q}_t$. The UFLS loss R_1 of the system is obtained by

$$R_1=\sum_{t=1}^{96}R_{1,t}^{\mathrm{load}} \tag{27}$$

According to the CVaR theory and the discrete characteristic of the disturbance set, cost term $R_{1,t}^{\mathrm{load}}$ is written as

$$R_{1,t}^{\mathrm{load}}=\alpha_{1,t}+\frac{1}{1-\beta_{1,t}}\sum_{q_t=1}^{\mathrm{Q}_t}\left[pr\left(\Delta P_{\mathrm{L},t}^{q_t}\right)\left(C_{1,t}^{q_t,\mathrm{load}}-\alpha_{1,t}\right)^+\right] \tag{28}$$

where

$$\left(C_{1,t}^{q_t,\mathrm{load}}-\alpha_{1,t}\right)^+=\max\left\{C_{1,t}^{q_t,\mathrm{load}}-\alpha_{1,t},0\right\} \tag{29a}$$

$$\Delta P_{1,t}^{q_t,\mathrm{load}}=\mathrm{LOSS}_k^{q_t}P_{\mathrm{D},t} \tag{29b}$$

$$C_{1,t}^{q_t,\mathrm{load}}=c^{\mathrm{load}}\Delta P_{1,t}^{q_t,\mathrm{load}}\Delta t \tag{29c}$$

In (28), $\alpha_{1,t}$ is the minimum VaR when the cumulative probability of the disturbance set exceeds the given confidence level $\beta_{1,t}$, which is the loss of load shedding in period t in this study. The second term on the right-hand side describes the average loss of load shedding of the system beyond $\beta_{1,t}$.

Here this work ignores the frequency regulation effect of the load. The UFLS value $\Delta P_{1,t}^{q_t,\mathrm{load}}$ is in (29b), which leads to loss expressed in (29c). $\mathrm{LOSS}_k^{q_t}$ is a piecewise function of $f_t^{q_t,\mathrm{nadir}}$, which represents the percentage of load shedding in the k-th round of UFLS. Term $f_t^{q_t,\mathrm{nadir}}$ is the frequency nadir under step disturbance $\Delta P_{\mathrm{L},t}^{q_t}$, which is obtained by

$$f_t^{q_t,\mathrm{nadir}}=f_0-\frac{\Delta P_{\mathrm{L},t}^{q_t}}{2P_b\left(\sum_{i=1}^{\mathrm{N}}X_{i,t}^{q_t}+K_{\mathrm{B},t}^{\mathrm{PFR}}\Big/P_b\right)} \tag{30}$$

where $X_{i,t}^{q_t}$ is the ramp gain of generation unit i [43]. The response time of the LS-BESS is extremely short, so its ramp gain can be approximated by a droop coefficient.

The above analysis was presented for the PFR capability of the system, and the decision variables are $\alpha_{1,t}$ and $P_{\mathrm{S},t}^{\mathrm{PFR}}$. Term $RoCoF^{0^+}$ is restricted so it is not too large for maintaining the IFR capability, to prevent triggering the UFLS relay before PFR has time to act. To do this, the worst-case scenario of disturbances is taken as the critical threshold of the hard constraint (14). According to formulas (13) and (14), $H_{\mathrm{S},t}$ satisfies the following relation:

$$H_{\mathrm{S},t}\geq\frac{\Delta P_{\mathrm{L},t}^{\mathrm{Q}_t}f_0}{2RoCoF^{\max}P_b} \tag{31}$$

2) R_2: This loss is calculated as

$$R_2=\sum_{t=1}^{96}\left(R_{2,t}^{\mathrm{wind}}+R_{2,t}^{\mathrm{load}}\right) \tag{32}$$

Term $\Delta P_{\mathrm{W},t}^{\mathrm{act}}$ satisfies the normal distribution with zero mean in period t [44,45], and its PDF is given by

$$\mathrm{PDF}\left(\Delta P_{\mathrm{W},t}^{\mathrm{act}}\right)=\frac{1}{\sigma_t\sqrt{2\pi}}\exp\left(-\frac{\left(\Delta P_{\mathrm{W},t}^{\mathrm{act}}\right)^2}{2{\sigma_t}^2}\right) \tag{33}$$

where σ_t is the standard deviation. According to three sigma guidelines, σ_t is set as

$$\sigma_t=\left(21\%P_{\mathrm{W},t}^{\mathrm{act}}\right)\Big/3 \tag{34}$$

Term $R_{2,t}^{\mathrm{wind}}$ is computed when wind power fluctuates above the forecasted value (i.e., $\Delta P_{\mathrm{W},t}^{\mathrm{act}}\geq 0$) as follows,

$$R_{2,t}^{\mathrm{wind}}=\alpha_{2,t}^{\mathrm{wind}}+\frac{1}{1-\beta_{2,t}^{\mathrm{wind}}}\int_0^{+\infty}\left(C_{2,t}^{\mathrm{wind}}-\alpha_{2,t}^{\mathrm{wind}}\right)^+\mathrm{PDF}\left(\Delta P_{\mathrm{W},t}^{\mathrm{act}}\right)d\left(\Delta P_{\mathrm{W},t}^{\mathrm{act}}\right) \tag{35}$$

where

$$\Delta P_{2,t}^{\mathrm{wind}}=\max\left\{\Delta P_{\mathrm{W},t}^{\mathrm{act}}-\left(\widehat{P}_{\mathrm{W},t}-P_{\mathrm{W},t}\right),0\right\} \tag{36a}$$

$$C_{2,t}^{\mathrm{wind}}=c_{\mathrm{W}}\Delta P_{2,t}^{\mathrm{wind}}\Delta t \tag{36b}$$

Term $\alpha_{2,t}^{\text{wind}}$ is the minimum VaR when the cumulative distribution function $\Phi(\Delta P_{\text{W},t}^{\text{act}})$ satisfies $\Phi(\Delta P_{\text{W},t}^{\text{act}}) \geq \beta_{2,t}^{\text{wind}}$ under the confidence level $\beta_{2,t}^{\text{wind}}$. This is the wind power curtailment loss that the system can tolerate due to upward fluctuations. In (36a), $\Delta P_{2,t}^{\text{wind}}$ represents the value of wind power curtailment, and its corresponding cost $C_{2,t}^{\text{wind}}$ is described in (36b).

Term $R_{2,t}^{\text{load}}$ is computed when $\Delta P_{\text{W},t}^{\text{act}} \leq 0$ as follows,

$$R_{2,t}^{\text{load}} = \alpha_{2,t}^{\text{load}} + \frac{1}{1-\beta_{2,t}^{\text{load}}} \int_{-\infty}^{0} \left(C_{2,t}^{\text{load}} - \alpha_{2,t}^{\text{load}}\right)^{+} \text{PDF}\left(\Delta P_{\text{W},t}^{\text{act}}\right) d\left(\Delta P_{\text{W},t}^{\text{act}}\right) \tag{37}$$

where

$$\Delta P_{2,t}^{\text{load}} = \max\left\{\breve{P}_{\text{W},t} - \left(P_{\text{W},t}^{\text{act}} + \Delta P_{\text{W},t}^{\text{act}}\right), 0\right\} \tag{38a}$$

$$C_{2,t}^{\text{load}} = c^{\text{load}} \Delta P_{2,t}^{\text{load}} \Delta t \tag{38b}$$

Formulas (37) and (38) are constrained by $\Phi(\Delta P_{\text{W},t}^{\text{act}}) \leq 1 - \beta_{2,t}^{\text{load}}$, and related descriptions about the loss of load shedding are similar to the above.

3) R_3: This variable can be directly described as

$$R_3 = \sum_{t=1}^{96} c_{\text{W}} \left(P_{\text{W},t}^{\text{act}} - P_{\text{W},t}\right) \Delta t \tag{39}$$

5. Solving method and numerical results

5.1. Solving method of the day-ahead model

The objective function and constraints established in this study contain nonlinear terms, which limits the effectiveness of solving methods using standard commercial optimization tools. Hence, it is necessary to perform piecewise linearization of the nonlinear terms. The nonlinear terms include (3c)–(3e), (12), (35), and (37), which can be transformed by piecewise linearization and McCormick linearization [46–48]. The transformation methods used in (3c)–(3e) were adopted from Ref. [46]. Details are shown below.

1) Equation (12): Let $s_{i,t} = u_{i,t} P_{g,i,t}$, and (12) can be equivalently expressed as

$$u_{i,t} P_{g,i}^{\min} \leq s_{i,t} \leq u_{i,t} P_{g,i}^{\max} \tag{40a}$$

$$0 \leq P_{g,i,t} - s_{i,t} \leq \left(1 - u_{i,t}\right) P_{g,i}^{\max} \tag{40b}$$

2) Equation (35): Let

$$I_{2,t}^{\text{wind}} = \frac{1}{1-\beta_{2,t}^{\text{wind}}} \int_{0}^{+\infty} \left(C_{2,t}^{\text{wind}} - \alpha_{2,t}^{\text{wind}}\right)^{+} \text{PDF}\left(\Delta P_{\text{W},t}^{\text{act}}\right) d\left(\Delta P_{\text{W},t}^{\text{act}}\right) \tag{41}$$

Suppose that a new set of binary variables o_t satisfy the following conditions,

$$o_t = \begin{cases} 1, & \text{if } C_{2,t}^{\text{wind}} \leq \alpha_{2,t}^{\text{wind}} \\ 0, & \text{if } C_{2,t}^{\text{wind}} > \alpha_{2,t}^{\text{wind}} \end{cases} \tag{42}$$

Equation (42) can be characterized as the following equivalent linear inequality,

$$\frac{\alpha_{2,t}^{\text{wind}} - C_{2,t}^{\text{wind}}}{\text{L}} < o_t \leq 1 + \frac{\alpha_{2,t}^{\text{wind}} - C_{2,t}^{\text{wind}}}{\text{L}} \tag{43}$$

where L is a sufficiently large positive number. So, we can obtain the following constraint,

$$0 \leq I_{2,t}^{\text{wind}} \leq (1 - o_t)\text{L} \tag{44}$$

Term $I_{2,t}^{\text{wind}}$ is non-zero if and only if $C_{2,t}^{\text{wind}} > \alpha_{2,t}^{\text{wind}} > 0$. According to the numerical characteristics of the normal distribution, $\text{PDF}(\Delta P_{\text{W},t}^{\text{act}})$ can be piecewise linearized in the range of $C_{2,t}^{\text{wind}} \geq \alpha_{2,t}^{\text{wind}}$, and the number of segments is set to 1. Further, the integral term is calculated, and we have

$$I_{2,t}^{\text{wind}} = \frac{1}{1-\beta_{2,t}^{\text{wind}}} \left\{0.069 \left[c_{\text{W}} \left(P_{\text{W},t} - \widehat{P}_{\text{W},t}\right) \Delta t - \alpha_{2,t}^{\text{wind}}\right] + 0.01 c_{\text{W}} P_{\text{W},t}^{\text{act}} \Delta t\right\} \tag{45}$$

3) Equation (37): Its treatment method is similar to (35). Let $I_{2,t}^{\text{load}} = \frac{1}{1-\beta_{2,t}^{\text{load}}} \int_{-\infty}^{0} (C_{2,t}^{\text{load}} - \alpha_{2,t}^{\text{load}})^{+} \text{PDF}(\Delta P_{\text{W},t}^{\text{act}}) d(\Delta P_{\text{W},t}^{\text{act}})$, and a new set of binary variables ς_t are defined by

$$\frac{\alpha_{2,t}^{\text{load}} - C_{2,t}^{\text{load}}}{\text{L}} < \varsigma_t \leq 1 + \frac{\alpha_{2,t}^{\text{load}} - C_{2,t}^{\text{load}}}{\text{L}} \tag{46}$$

So, we can have

$$0 \leq I_{2,t}^{\text{load}} \leq (1 - \varsigma_t)\text{L} \tag{47}$$

Similarly, term $I_{2,t}^{\text{load}}$ is approximately transformed by

$$I_{2,t}^{\text{load}} = \frac{1}{1-\beta_{2,t}^{\text{load}}} \left\{0.069 \left[c^{\text{load}} \left(\breve{P}_{\text{W},t} - P_{\text{W},t}^{\text{act}}\right) \Delta t - \alpha_{2,t}^{\text{load}}\right] + 0.01 c^{\text{load}} P_{\text{W},t}^{\text{act}} \Delta t\right\} \tag{48}$$

The essence of the RO approach based on the budget uncertainty set is to obtain the optimal decision when the uncertain variable is at the worst value. When adopting this approach to tackle the uncertainty of wind power over a large timescale, the optimization goal of the day-ahead dispatch becomes a double-layer nested problem of the form "min-max". The general transformation form of this RO model is characterized as

$$\text{minimize} \quad C^{\text{DA}} = \ldots + \max \sum_{t=1}^{96} k_t z_{\text{W},t} \tag{49}$$

where k_t are a set of coefficients.

The decision variables of the inner optimization problem are the uncertainty variables of the outer problem. If the inner layer "max" is not transformed, (49) cannot be solved. Duality theory provides a feasible method for the transformation [49]. The constraints associated with $z_{\text{W},t}$ are shown as follows,

$$\left|z_{\text{W},t}\right| \leq 1 \tag{50a}$$

$$z_{\text{W},t} \geq \frac{1}{P_{\text{W},t}^{\text{h}}} \left(P_{\text{W},t} - P_{\text{W},t}^{\text{pre}}\right) \tag{50b}$$

$$\sum_{t=1}^{96} \left|z_{\text{W},t}\right| \leq \Gamma_{\text{W}} \tag{50c}$$

where (50b) is transformed by (9), and $P_{\text{W},t}^{\text{h}} = \left(P_{\text{W},t}^{\max} - P_{\text{W},t}^{\min}\right)/2$. Inequalities (50a)–(50c) are the constraints of the inner-layer optimization problem.

Let $z_{\text{W},t}^{+}$ and $z_{\text{W},t}^{-}$ be the orthogonal projections of $z_{\text{W},t}$ and $-z_{\text{W},t}$ on the non-negative quadrant, respectively; that is,

$$z_{\text{W},t}^{+} = \max\left\{z_{\text{W},t}, 0\right\} \tag{51a}$$

$$z_{\text{W},t}^{-} = \max\left\{-z_{\text{W},t}, 0\right\} \tag{51b}$$

Further, we have

$$z_{\text{W},t} = z_{\text{W},t}^{+} - z_{\text{W},t}^{-} \tag{52a}$$

$$\left|z_{\text{W},t}\right| = z_{\text{W},t}^{+} + z_{\text{W},t}^{-} \tag{52b}$$

Therefore, the inner-layer problem can be rewritten as,

$$\max \sum_{t=1}^{96} k_t \left(z_{\mathrm{W},t}^{+} - z_{\mathrm{W},t}^{-}\right) \tag{53a}$$

$$\text{s.t.} \quad z_{\mathrm{W},t}^{+} + z_{\mathrm{W},t}^{-} \leq 1 \tag{53b}$$

$$-z_{\mathrm{W},t}^{+} + z_{\mathrm{W},t}^{-} \leq \frac{1}{P_{\mathrm{W},t}^{\mathrm{fh}}}\left(P_{\mathrm{W},t}^{\mathrm{pre}} - P_{\mathrm{W},t}\right) \tag{53c}$$

$$\sum_{t=1}^{96} \left(z_{\mathrm{W},t}^{+} + z_{\mathrm{W},t}^{-}\right) \leq \Gamma_{\mathrm{W}} \tag{53d}$$

$$z_{\mathrm{W},t}^{+}, z_{\mathrm{W},t}^{-} \geq 0 \tag{53e}$$

The corresponding dual problem of (53) is described by

$$\min \left\{ \sum_{i=1}^{96} \left[\lambda^{(i)} + \frac{1}{P_{\mathrm{W},i}^{\mathrm{fh}}} \left(P_{\mathrm{W},i}^{\mathrm{pre}} - P_{\mathrm{W},i}\right)\sigma^{(i)} \right] + \Gamma_{\mathrm{W}}\delta \right\} \tag{54a}$$

$$\text{s.t.} \quad \lambda^{(i)} - \sigma^{(i)} + \delta \geq k_t \tag{54b}$$

$$\lambda^{(i)} + \sigma^{(i)} + \delta \geq -k_t \tag{54c}$$

$$\lambda^{(i)} \geq 0, \quad \sigma^{(i)} \geq 0, \quad \delta \geq 0 \tag{54d}$$

where $\lambda^{(i)}$, $\sigma^{(i)}$, and δ are the variables introduced for solving the dual problem.

The optimization model established in this study is now a mixed integer linear programming (MILP) model, which is solved in MATLAB by calling the YALMIP toolbox in CPLEX solver.

5.2. Case data

This work takes the typical ten-unit system described in Ref. [50] as the base case, and makes the following modifications: replace U5 and U6 with wind power generators with a capacity of 950MW, where the installed ratio of wind power to thermal power in the system is about 40:60. In addition, a 200MW/800MWh LS-BESS is connected to the power grid. A simple diagram of the test system is shown in Fig. 2. It is a scaled-down power system with negligible power transmission loss. Parameter f^{db} of generation units is 0.033Hz, $\Delta f^{\max}$ is 0.2Hz, and c_g^{DPR1} and c_g^{DPR2} are 60$/MWh and 150$/MWh. U2, U4, U7, and U8 can participate in SFR. For the LS-BESS, $c_{\mathrm{B},op}$ is set as 30$/MWh, $c_{\mathrm{B}}^{\mathrm{FFR}}$ and $c_{\mathrm{B}}^{\mathrm{PFR}}$ are 60$/MWh, η_{ch}=η_{dis}=95%, $\mathrm{SoC}_{\mathrm{B}}^{\mathrm{ini}}$=50%, $\mathrm{SoC}_{\mathrm{B}}^{\min}$=10%, and $\mathrm{SoC}_{\mathrm{B}}^{\max}$=90%. Other parameters of generation units [46] are listed in Table 1. The forecasted wind power and output ranges [51] and system load demand [46] are shown in Fig. 3.

For the power system frequency, this work sets f_0 to 50Hz, $RoCoF^{\max}$=0.5Hz/s, and $f^{\min}$=49.5Hz [10]. The probability statistics of the system having stepped disturbances are shown in Table 2, where the disturbance values are given in the form of per unit value. This load increase can either be caused by the increase in power consumption or a line disconnection, 12% equivalent load increase means the load increases by 12%P_b. The frequencies of stepwise UFLS are 49.5Hz, 49.3Hz, 49.1Hz, and 48.9Hz, and the corresponding load loss is 7% [52]. The

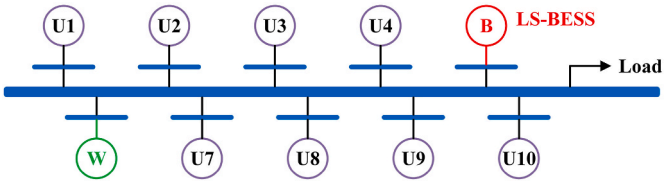

Fig. 2. A simple diagram of the modified ten-unit power system with a wind power generator and a LS-BESS.

average HF_t value of 24 representative days is adopted and modified from Ref. [53], which is shown in Fig. 4. The unit compensation price of the system for the generators participating in SFR is 9$/MWh, c_{W}=100 $/MWh [54], and c^{load}=200$/MWh [55]. This work sets ξ_1=2, ξ_2=1, ξ_3=0.8, β_1=99.99%, β_2^{wind}=β_2^{load}=95%, γ=8%, and Γ_{W}=32 in the optimization model. The online generation unit in the initial period on the dispatch day is U2.

5.3. Optimization results and discussions

1) Optimization results: The simulation of the proposed model runs for 4160s on a 4-core, 3.60GHz AMD Ryzen3 3200G with Radeon Vega Graphics processor. Numerically, the C^{DA} obtained by the proposed scheme is $737.15K, and the resulting day-ahead dispatch strategies are shown in Fig. 5.

2) For the first type of FCAS: The spaces of the LS-BESS participating in various FCASs are shown in Fig. 5(a). It can be seen that the LS-BESS needs to reserve a large margin in the first 32 steps to support possible large step disturbances, to maintain sufficient IFR capability of the system. This is because the total inertia of the online generation units in these periods is low, which is not enough to meet the security constraint in (14). After the 33rd period, the inertia of generation units becomes sufficient, and thus the LS-BESS has reduced reserve space for participating in FFR. The reserved PFR strategy of the LS-BESS shown in Fig. 5 (a) can make the system resist 12% of step disturbance in the first period. But if the disturbance is 15%, the frequency nadir drops to 49.375Hz, and UFLS occurs with a value of 49MW. In other periods, the frequency nadir does not trigger the UFLS relay after being disturbed by 15% due to higher generation units' capacities.

If the LS-BESS does not reserve PFR under the generation units power output shown in Fig. 5(b), the system can only resist 5% of step disturbance throughout periods 1–20, and 8% in periods 21–32, and 10% in periods 88–96, which is potentially risky for the dispatch mechanism. Particularly, for periods 1–12, once a 15% disturbance occurs, all rounds of UFLS are triggered, which seriously affects the security of operation and significantly increases the loss of the system. Therefore, when frequency reliability is considered, the LS-BESS can enhance the security degree of the system. More reserve spaces of the LS-BESS are dispatched when online units' capabilities are insufficient; otherwise, its regulation amount is small or even zero.

3) For the second type of FCAS: Fig. 5(a), (c), and (d) show that the reserved SFR of the LS-BESS and generation units. The total reserved SFR cost on the dispatch day is $48K. SFR generators need to reserve some spaces in each period to cope with the fixed load and unexpected wind power fluctuations. The interval acceptance strategy for wind power is shown in Fig. 5(e). To cope with possible upward fluctuations, some spaces for lower SFR are reserved in day-ahead scheduling, which can enhance the acceptance capacity of wind power, except in periods 77–81 when the RO approach based on the budget uncertainty set conservatively calculates $P_{\mathrm{W},t}^{\mathrm{act}}$ to be 0, and the system does not have a lower SFR bound. If the actual wind power within the period is higher than $P_{\mathrm{W},t}$ when downward fluctuations occur, it is not necessary to have some reserve for the upper SFR because such disturbances cannot cause the load shedding, such as in periods 1–8. It can be seen from Fig. 5(e) that the acceptance values of wind power change from a single curve to a band, and the reserved upper and lower SFR spaces can make the grid have the flexibility to accept any wind power in the band. Compared to only accepting the wind power benchmark, the interval strategy improves wind power acceptance and enhances the flexibility of power system operations.

4) For the third type of FCAS: The discharging of the LS-BESS can meet the load demand in the power system with generation units and wind power generator. The charging scheduling of the LS-BESS can achieve three functions: 1) it can prevent some units from entering the deep peak regulation state as much as possible, such as in periods 89–93;

Table 1
Parameters of generation units.

Parameters	U1	U2	U3	U4	U7	U8	U9	U10
$c_{g,i}^{on}$, $c_{g,i}^{off}$ ($)	4500	5000	550	560	260	30	30	30
a_i ($/MW^{2}h)	0.00048	0.00031	0.00200	0.00211	0.00079	0.00413	0.00222	0.00173
b_i ($/MWh)	16.19	17.26	16.60	16.50	27.74	25.92	27.27	27.79
c_i ($/h)	1000	970	700	680	480	660	665	670
T_i^{on}, T_i^{off} (Δt)	32	32	20	20	12	4	4	4
$P_{g,i}^{max}$ (MW)	455	455	130	130	85	55	55	55
$P_{g,i}^{min}$ (MW)	150	150	20	20	25	10	10	10
$V_{g,i}^{+}$, $V_{g,i}^{-}$ (MW/15mins)	50	50	20	20	20	15	15	15
H_i (s)	9.3	9.3	8.1	8.1	5.8	5.8	5.8	5.8
$K_{g,i}^{PFR}$ (p.u.)	25	25	20	20	17	17	17	17
$T_{g,i}$ (s)	8.0	8.0	7.2	7.2	6.0	6.0	6.0	6.0

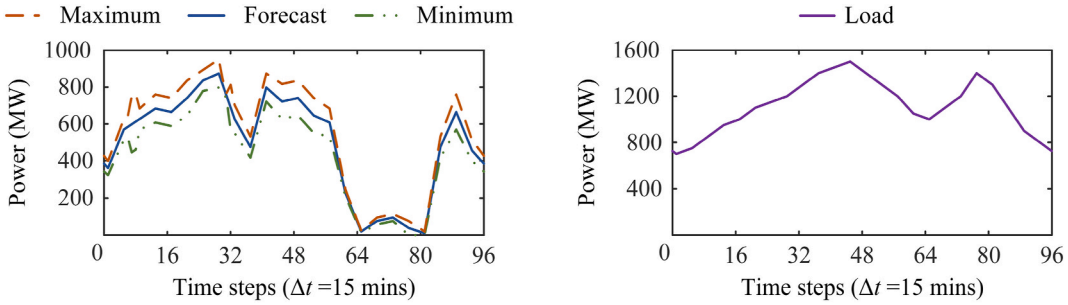

(a) Wind power (b) Load demand

Fig. 3. Relevant data of wind power and load.

Table 2
Step disturbance values and their probabilities.

$\Delta P_{L,t}$ (p.u.)	Probabilities	$\Delta P_{L,t}$ (p.u.)	Probabilities	$\Delta P_{L,t}$ (p.u.)	Probabilities	$\Delta P_{L,t}$ (p.u.)	Probabilities	$\Delta P_{L,t}$ (p.u.)	Probabilities
<1%	0.94850	1%	0.02000	3%	0.01500	5%	0.01000	7%	0.00500
8%	0.00100	10%	0.00030	12%	0.00010	15%	0.00008	>15%	0.00002

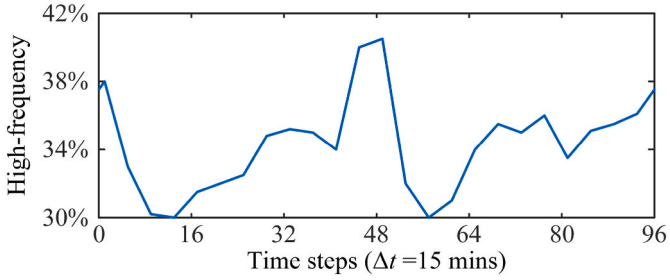

Fig. 4. Ratios of high-frequency components in non-step disturbances.

2) it can expand capacity for frequency responses that need to discharge in a time period, such as in periods 1–12; and 3) it can reserve electric energy for itself, such as in periods 94–96. The LS-BESS's SoC is shown in Fig. 5(f), and its total cost accounts for 21.01% of C^{DA}.

5.4. Comparison of different dispatch schemes

This work compares the control scheme described in Section 5.3 with the following five schemes.

- Scheme 1: ξ_1=1, ξ_2=1, ξ_3=1 (as in (6)).
- Scheme 2: ξ_1=0.8, ξ_2=1, ξ_3=2.
- Scheme 3: ξ_1=0, ξ_2=0, ξ_3=0.8.
- Scheme 4: Without interval acceptance strategy of wind power.
- Scheme 5: Various values of Γ_W.

1) The impact of risk preference degree: The first three comparison schemes are employed to analyze the impact of different risk aversion coefficients (see (6)) of grid operators on the dispatch. In Scheme 1, the system can only resist a large step disturbance with a magnitude of 12% in the first period. The system in Scheme 2 is relatively weak, the frequency nadir drops to 49.44Hz with a 12% disturbance in the first period, which causes a round of UFLS in normal operations within the confidence level of $\beta_{1,t}$=99.99%. This scheme allows up to 49MW of load shedding. Table 3 lists the comparison results of some economic indicators in the first three schemes. It can be seen that the operation cost of generation units is the largest when the frequency security is emphasized. This is because generation units with stronger frequency response ability are preferentially dispatched, and such generation units generally have a larger power capacity and higher operation cost. The LS-BESS's cost for participating in PFR in the control scheme is lowest, which is highest in Scheme 1 in order to make up for the insufficient capacity of generation units. From the control scheme, Scheme 1, to Scheme 2, operators pay more attention to the impact of non-step disturbances, so the costs of SFR reserved by generation units and the LS-BESS gradually rises.

In Scheme 3, operators do not consider the risk caused by power deficiencies and fluctuations, so the LS-BESS does not reserve more PFR and SFR. When step disturbances occur, the frequency nadir points in each period are shown in Fig. 6. The PFR capability of the entire system depends on generation units in this scheme, which makes it only able to

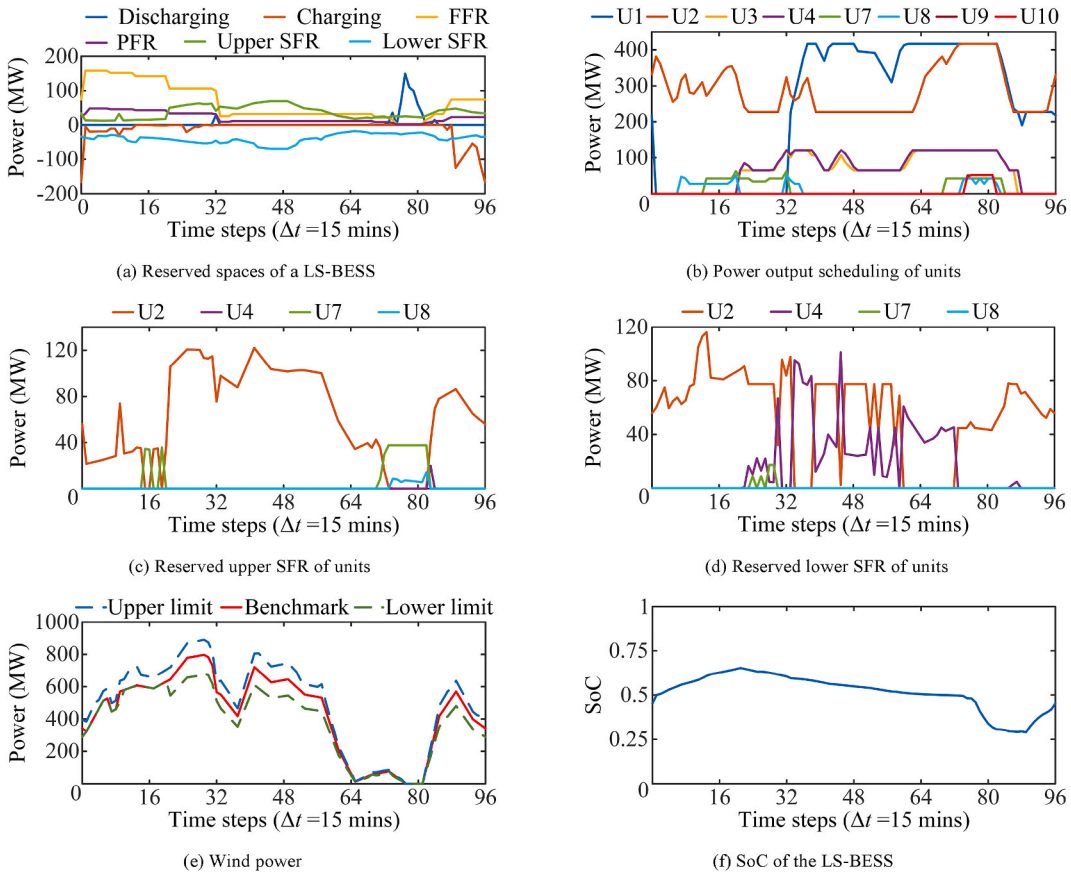

Fig. 5. Day-ahead dispatch strategies of the modified ten-unit system.

Table 3
Comparison of cost indicators in three schemes.

Parameters	Control scheme	Scheme 1	Scheme 2
$C_{g,op}$	$371.41k	$370.01k	$370.14k
C_B^{PFR}	$30.15k	$30.30k	$30.24k
C_B^{SFR}	$16.52k	$16.71k	$16.73k
C_g^{SFR}	$31.48k	$31.78k	$31.81k

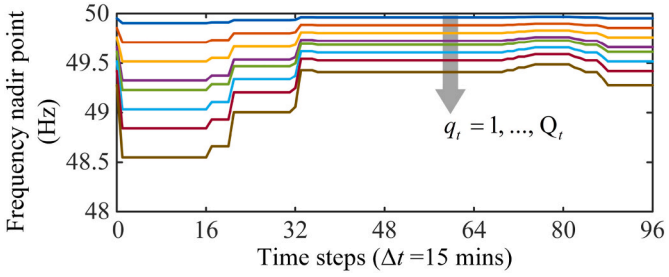

Fig. 6. The frequency nadir points in Scheme 3.

resist 5% step disturbances in the first 20 periods. Even after the generation units' capacities are fully released, a round of UFLS still occurs with a 15% disturbance. Results show that the loss of UFLS in this scheme reaches $588.92k. The wind power benchmark obtained in this scheme is the same as our strategy, but there are no additional SFR spaces for upward and downward fluctuations. Hence, the acceptance of wind power of the system is a single curve, not an interval. The reserved SFR cost that can be saved is $23.61k, but the potential loss is as high as $272.23k.

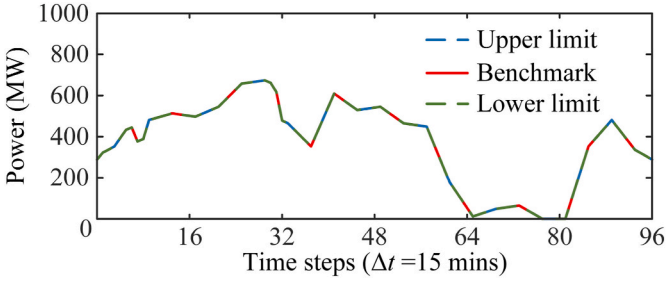

Fig. 7. Acceptance value of wind power in Scheme 4.

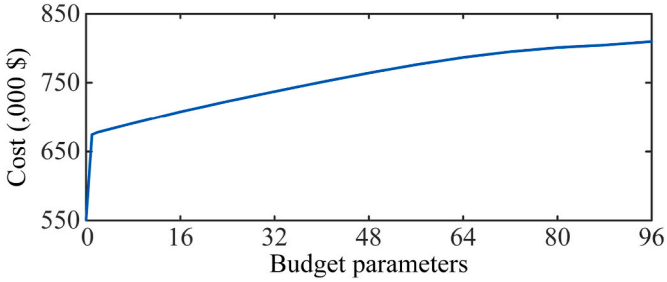

Fig. 8. C^{DA} under different budget parameters.

2)Importance of interval acceptance strategy: The acceptance strategy of wind power in Scheme 4 is shown in Fig. 7, which cannot cope with the unexpected fluctuations within the period. Since c^{load} is greater than c_W, operators are more inclined to avoid the downward fluctuations

of wind power, which leads to the acceptance value of wind power being lower than the control scheme. Lower wind power increases the power generation from generation units and the LS-BESS, which increases the operation cost by 8.07% compared with the control scheme. The reserved SFR by the LS-BESS and generation units in Scheme 4 can only cope with the fixed load fluctuations. Although the reserved cost is reduced, the risk is significantly deteriorated, which makes C^{DA} increase by 25.91% compared to the control scheme.

3)Sensitivity analysis of robust parameters: Term Γ_W determines the conservatism of the RO approach based on the budget uncertainty set. When Γ_W=0, the uncertainty disappears, and the predicted wind power is assumed to be the same as its actual value, which undermines the robustness in the real-time operations. Any changes may make the dispatch decisions invalid. Fig. 8 illustrates the impacts of the changes of Γ_W on C^{DA}. It can be seen that as conservatism index or budget parameter increases, C^{DA} gradually increases. C^{DA} is the largest when Γ_W=96, and RO approach based on the budget uncertainty set degenerates into the standard RO. As seen from Fig. 8, as soon as uncertainty is considered in the model, the cost increases significantly, as illustrated by the sharp increase when the budget parameter is very small. When Γ_W=1, the cost value rises by 22.47% compared with Γ_W=0. This is expected because when uncertainty is considered, RO approach based on the budget uncertainty set makes decisions under the worst-case scenario, so that the robustness of the dispatch decision is ensured. In real-world day-ahead dispatch, grid operators can take Fig. 8 as a reference and select an appropriate Γ_W value for system costs.

6. Conclusions

For the complementarity and contradiction of three types of FCASs in this study, a day-ahead dispatch strategy for a power system with a LS-BESS and generation units has been proposed, which are coordinated to participate in multiple frequency regulation services. Comprehensive mathematical derivations and comparative studies have been conducted in this work, which is summarized as follows.

- The design principle of the day-ahead dispatch model is to minimize the operation costs of the power system, and the CVaR theory is adopted to effectively measure mitigate potential risks of the power system.
- For short-term wind power uncertainties, the proposed wind energy interval acceptance strategy can improve the flexibility of the power system. For long-term wind power uncertainties, the adopted RO approach based on the budget uncertainty set can better realize economic operations while ensuring the robustness for practical power system operations compared with the standard RO.
- A LS-BESS and generation units have complementary advantages to synergistically participate in multi-types FCASs through the proposed day-ahead dispatch strategy. As an effective method to compensate insufficient regulation capabilities and the limited ramping rate of generation units, using LS-BESSs can enhance the resilience, flexibility and peak regulation capacity of the power system.

This study contributes to secure, reliable, and economic operations of power systems and promotes the accelerated construction of the new type of power system dominated by renewable energy on the trajectory of achieving the goals of carbon peak and carbon neutrality.

In real-world power system operations, some of the most significant risks may also arise from the spatiotemporal dynamics of renewables and storage systems with transmission constraints, which have not been considered in the current power dispatch framework. In addition, the existing algorithms solved the dispatch model need to be improved to be applied to practical power systems. These aspects will fall in our future research.

Credit authors statement

Mingze Zhang: Conceptualization, Methodology, Data curation, and Writing – original draft. Weidong Li: Supervision, Conceptualization, Project administration, and Writing – review & editing. Samson Shenglong Yu: Supervision, Visualization, Writing – review & editing, and Resources. Haixia Wang: Investigation and Validation. Yu Ba: Software and Formal analysis.

Declaration of competing interest

The authors declare that they have no known competing financial interests or personal relationships that could have appeared to influence the work reported in this paper.

Data availability

The authors are unable or have chosen not to specify which data has been used.

Acknowledgements

This work was supported by the National Natural Science Foundation of China [grant number U22A20223]; and the Australian Research Council (ARC) [grant number IC210100021].

References

[1] Makolo P, Zamora R, Lie T-T. The role of inertia for grid flexibility under high penetration of variable renewables - a review of challenges and solutions. Renew Sustain Energy Rev 2021;147:111223. https://doi.org/10.1016/j.rser.2021.111223.
[2] Heylen E, Teng F, Strbac G. Challenges and opportunities of inertia estimation and forecasting in low-inertia power systems. Renew Sustain Energy Rev 2021;147:111176. https://doi.org/10.1016/j.rser.2021.111176.
[3] Sun Y, Bahrami S, Wong VWS, Lampe L. Chance-constrained frequency regulation with energy storage systems in distribution networks. IEEE Trans Smart Grid 2020;11(1):215–28.
[4] Hong Z, Wei Z, Li J, Han X. A novel capacity demand analysis method of energy storage system for peak shaving based on data-driven. J Energy Storage 2021;39:102617. https://doi.org/10.1016/j.est.2021.102617.
[5] Fang Y, Zhao S, Chen Z. Multi-objective unit commitment of jointly concentrating solar power plant and wind farm for providing peak-shaving considering operational risk. Int J Electr Power Energy Syst 2022;137:107754. https://doi.org/10.1016/j.ijepes.2021.107754.
[6] Xie R, Wei W, Li M, Dong Z, Mei S. Sizing capacities of renewable generation, transmission, and energy storage for low-carbon power systems: a distributionally robust optimization approach. Energy 2023;263:125653. https://doi.org/10.1016/j.energy.2022.125653.
[7] Chen S, Li Z, Li W. Integrating high share of renewable energy into power system using customer-sited energy storage. Renew Sustain Energy Rev 2021;143:110893. https://doi.org/10.1016/j.rser.2021.110893.
[8] Akram U, Nadarajah M, Shah R, Milano F. A review on rapid responsive energy storage technologies for frequency regulation in modern power systems. Renew Sustain Energy Rev 2020;120:109626. https://doi.org/10.1016/j.rser.2019.109626.
[9] Pusceddu E, Zakeri B, Gissey GC. Synergies between energy arbitrage and fast frequency response for battery energy storage systems. Appl Energy 2021;283:116274. https://doi.org/10.1016/j.apenergy.2020.116274.
[10] Wen Y, Li W, Huang G, Liu X. Frequency dynamics constrained unit commitment with battery energy storage. IEEE Trans Power Syst 2016;31(6):5115–25.
[11] Ali L, Muyeen SM, Bizhani H, Ghosh A. Optimal planning of clustered microgrid using a technique of cooperative game theory. Elec Power Syst Res 2020;183:106262. https://doi.org/10.1016/j.epsr.2020.106262.
[12] Sharma V, Cortes A, Cali U. Use of forecasting in energy storage applications: a review. IEEE Access 2021;9:114690–704.
[13] Hanif S, Alam MJE, Roshan K, Bhatti BA, Bedoya JC. Multi-service battery energy storage system optimization and control. Appl Energy 2022;311:118614. https://doi.org/10.1016/j.apenergy.2022.118614.
[14] Wen K, Li W, Yu SS, Li P, Shi P. Optimal intra-day operations of behind-the-meter battery storage for primary frequency regulation provision: a hybrid lookahead method. Energy 2022;247:123482. https://doi.org/10.1016/j.energy.2022.123482.
[15] Li X, Ma R, Yan S, Wang S, Yang D, Xu S, et al. Multi-timescale cooperated optimal dispatch strategy for ultra-large-scale storage system. Energy Rep 2020;6:1–8. https://doi.org/10.1016/j.egyr.2020.10.026.

[16] Zheng M, Wang X, Meinrenken CJ, Ding Y. Economic and environmental benefits of coordinating dispatch among distributed electricity storage. Appl Energy 2018; 210:842–55. https://doi.org/10.1016/j.apenergy.2017.07.095.
[17] Nasrolahpour E, Kazempour J, Zareipour H, Rosehart WD. A bilevel model for participation of a storage system in energy and reserve markets. IEEE Trans Sustain Energy 2018;9(2):582–98.
[18] Xu B, Wang Y, Dvorkin Y, Fernández-Blanco R, Silva-Monroy CA, Watson J-P, et al. Scalable planning for energy storage in energy and reserve markets. IEEE Trans Power Syst 2017;32(6):4515–27.
[19] Wang X, Ying L, Wen K, Lu S. Bi-level non-convex joint optimization model of energy storage in energy and primary frequency regulation markets. Int J Electr Power Energy Syst 2022;134:107408. https://doi.org/10.1016/j.ijepes.2021.107408.
[20] Zhang M, Li W, Yu SS, Wen K, Muyeen SM. Day-ahead optimization dispatch strategy for large-scale battery energy storage considering multiple regulation and prediction failures. Energy 2023;270:126945. https://doi.org/10.1016/j.energy.2023.126945.
[21] Khalilisenobari R, Wu M. Optimal participation of price-maker battery energy storage systems in energy and ancillary services markets considering degradation cost. Int J Electr Power Energy Syst 2022;138:107924. https://doi.org/10.1016/j.ijepes.2021.107924.
[22] Dhople SV, Chen YC, DeVille L, Domínguez-García AD. Analysis of power system dynamics subject to stochastic power injections. IEEE Trans Circuits Syst I: Reg Papers 2013;60(12):3341–53.
[23] Hosseini SA, Toubeau J-F, Grève ZD, Vallée F. An advanced day-ahead bidding strategy for wind power producers considering confidence level on the real-time reserve provision. Appl Energy 2020;280:115973. https://doi.org/10.1016/j.apenergy.2020.115973.
[24] Li J, Zhou J, Chen B. Review of wind power scenario generation methods for optimal operation of renewable energy systems. Appl Energy 2020;280:115992. https://doi.org/10.1016/j.apenergy.2020.115992.
[25] Gutierrez-Garcia F, Arcos-Vargas A, Gomez-Exposito A. Robustness of electricity systems with nearly 100% share of renewables: a worst-case study. Renew Sustain Energy Rev 2022;155:111932. https://doi.org/10.1016/j.rser.2021.111932.
[26] Khojasteh M, Faria P, Vale Z. A robust model for aggregated bidding of energy storages and wind resources in the joint energy and reserve markets. Energy 2022; 238:121735. https://doi.org/10.1016/j.energy.2021.121735.
[27] Bertsimas D, Sim M. The price of robustness. Oper Res 2004;52(1):35–53.
[28] Dai X, Li Y, Zhang K, Feng W. A robust offering strategy for wind producers considering uncertainties of demand response and wind power. Appl Energy 2020; 279:115742. https://doi.org/10.1016/j.apenergy.2020.115742.
[29] Liu F, Bie Z, Liu S, Ding T. Day-ahead optimal dispatch for wind integrated power system considering zonal reserve requirements. Appl Energy 2017;188:399–408. https://doi.org/10.1016/j.apenergy.2016.11.102.
[30] Rajagopal R, Bitar E, Varaiya P, Wu F. Risk-limiting dispatch for integrating renewable power. Int J Electr Power Energy Syst 2013;44(1):615–28. https://doi.org/10.1016/j.ijepes.2012.07.048.
[31] Wang B, Wang S, Zhou X, Watada J. Two-stage multi-objective unit commitment optimization under hybrid uncertainties. IEEE Trans Power Syst 2016;31(3): 2266–77.
[32] Yang H, Liang R, Yuan Y, Chen B, Xiang S, Liu J, et al. Distributionally robust optimal dispatch in the power system with high penetration of wind power based on net load fluctuation data. Appl Energy 2022;313:118813. https://doi.org/10.1016/j.apenergy.2022.118813.
[33] Mahmutoğulları Aİ, Ahmed S, Çavuş Ö, Aktürk MS. The value of multi-stage stochastic programming in risk-averse unit commitment under uncertainty. IEEE Trans Power Syst 2019;34(5):3667–76.
[34] Liu L, Li W, Ba Y, Shen J, Jin C, Wen K. An analytical model for frequency nadir prediction following a major disturbance. IEEE Trans Power Syst 2020;35(4): 2527–36.
[35] Farmer WJ, Rix AJ. Understanding the impact of network topology on frequency stability considering continuous spatial-temporal disturbances from wind generation. Int J Electr Power Energy Syst 2021;129:106776. https://doi.org/10.1016/j.ijepes.2021.106776.
[36] Wu J, Zhang B, Deng W, Zhang K. Application of cost-CVaR model in determining optimal spinning reserve for wind power penetrated system. Int J Electr Power Energy Syst 2015;66:110–5. https://doi.org/10.1016/j.ijepes.2014.10.051.
[37] Zhang Y, Wang J, Wang X. Review on probabilistic forecasting of wind power generation. Renew Sustain Energy Rev 2014;32:255–70. https://doi.org/10.1016/j.rser.2014.01.033.
[38] Du M, Niu Y, Hu B, Zhou G, Luo H, Qi X. Frequency regulation analysis of modern power systems using start-stop peak shaving and deep peak shaving under different wind power penetrations. Int J Electr Power Energy Syst 2021;125:106501. https://doi.org/10.1016/j.ijepes.2020.106501.
[39] Fernández-Muñoz D, Pérez-Díaz JI, Guisández I, Chazarra M, Fernández-Espina Á. Fast frequency control ancillary services: an international review. Renew Sustain Energy Rev 2020;120:109662. https://doi.org/10.1016/j.rser.2019.109662.
[40] Northeast China Energy Regulatory Bureau of National Energy Administration. Operation rules of northeast electric power ancillary service market. 2020. http://dbj.nea.gov.cn/zwfw/zcfg/202012/t20201223_4055300.html. [Accessed 16 October 2022].
[41] Zhang M, Tang Y, Liu L, Zhou D. Optimal investment portfolio strategies for power enterprises under multi-policy scenarios of renewable energy. Renew Sustain Energy Rev 2022;154:111879. https://doi.org/10.1016/j.rser.2021.111879.
[42] Rockafellar R, Uryasev S. Optimization of conditional value-at-risk. J Risk 2000;2 (3):21–41.
[43] Egido I, Fernandez-Bernal F, Centeno P, Rouco L. Maximum frequency deviation calculation in small isolated power systems. IEEE Trans Power Syst 2009;24(4): 1731–8.
[44] Ding Y, Shao C, Yan J, Song Y, Zhang C, Guo C. Economical flexibility options for integrating fluctuating wind energy in power systems: the case of China. Appl Energy 2018;228:426–36. https://doi.org/10.1016/j.apenergy.2018.06.066.
[45] Lin W, Wen J, Cheng S, Lee W. An investigation on the active-power variations of wind farms. IEEE Trans Ind Appl 2012;48(3):1087–94.
[46] Carrion M, Arroyo JM. A computationally efficient mixed-integer linear formulation for the thermal unit commitment problem. IEEE Trans Power Syst 2006;21(3):1371–8.
[47] Restrepo JF, Galiana FD. Unit commitment with primary frequency regulation constraints. IEEE Trans Power Syst 2005;20(4):1836–42.
[48] Deng L, Sun H, Li B, Sun Y, Yang T, Zhang X. Optimal operation of integrated heat and electricity systems: a tightening McCormick approach. Engineering 2021;7(8): 1076–86. https://doi.org/10.1016/j.eng.2021.06.006.
[49] Bertsekas D. Nonlinear programming. Belmont, MA, USA: Athena Sci; 1995.
[50] Kazarlis SA, Bakirtzis AG, Petridis V. A genetic algorithm solution to the unit commitment problem. IEEE Trans Power Syst 1996;11(1):83–92.
[51] Wei W, Liu F, Mei S. Robust and economical scheduling methodology for power systems—part two: application examples. Autom Electr Power Syst 2013;37(18): 60–7.
[52] Li C, Wu Y, Sun Y, Zhang H, Liu Y, Liu Y, et al. Continuous under-frequency load shedding scheme for power system adaptive frequency control. IEEE Trans Power Syst 2020;35(2):950–61.
[53] Hu Z, Xie X, Zhang F, Zhang J, Song Y. Research on automatic generation control strategy incorporating energy storage resources. Proc CSEE 2014;34(29):5080–7.
[54] Duan C, Jiang L, Fang W, Liu J. Data-driven affinely adjustable distributionally robust unit commitment. IEEE Trans Power Syst 2018;33(2):1385–98.
[55] Wang C, Liu F, Wang J, Qiu F, Wei W, Mei S, et al. Robust risk-constrained unit commitment with large-scale wind generation: an adjustable uncertainty set approach. IEEE Trans Power Syst 2017;32(1):723–33.